RECYCLED GABBRO SIGNATURE IN HOTSPOT MAGMAS UNVEILED BY PLUME-RIDGE INTERACTIONS

N. A. Stroncik[1] & C.W. Devey[2]

[1] GFZ Helmholtz Centre Potsdam, Telegrafenberg, D-14473 Potsdam, Germany

[2] Leibniz-Institut für Meereswissenschaften, Wischhofstr. 1-3, D-24148 Kiel, Germany

Intraplate melting anomalies ("plumes") interact with mid-ocean spreading centres over large distances, leading to changes in composition of both the intraplate and spreading axis magmas. There is no concensus on how the interaction occurs, with both pipe-like, channeled flow of either melt or mantle from the plume to the ridge and flow of material from the spreading centre to the plume being suggested [1-3]. Here we present He, Ne and Ar isotopes and trace-element data from the Foundation hotspot which we model to show that the ridge does not contribute magmas to the plume. Instead, when plume and ridge approach each other, deep plume melts containing most of the noble gases and trace elements derived from the peridoditic plume source are transferred to the ridge, bypassing the near-ridge seamounts. These seamounts then erupt magmas with ridge-like geochemistry but with geochemical anomalies (excesses in Sr, Pb) suggesting that their "ridge-like" signature results from melting of a recycled oceanic lower crust component in their source. Other near-ridge plumes (Easter, Galapagos, Iceland, 80 Ma Hawaii) also have this "recycled oceanic lower crust" signature, implying that removal of deep melts to the spreading axis unveils a previously undetected subduction component in plume sources.

In areas where hotspots are located close to mid-ocean ridges, the upwelling mantle flow ("plume") interacts with the spreading system producing along-axis bathymetric, gravitational and geochemical anomalies [4,5]. Large volcanic features, such as the Kerguelen or the Ontong Java Plateau, are thought to be remnants of extreme hot spot activity at or near an ancient mid-ocean ridge [6]. Despite the importance of such plume-ridge interaction for plate production, there is no consensus on how or especially in what physical form material transfer from plume to ridge occurs (see review by e.g. [1]). Numerical models predict either unidirectional pipeline-like or radial flow of either solid or molten plume material e.g. [2,3]. Compositional changes observed in near-axis plume volcanics have led geochemists, in contrast, to suggest two-way plume-ridge interaction e.g. [7,8]. Here we show, primarily using noble gas and trace element evidence from the age-progressive Foundation Seamount Chain, that enriched (probably carbonatitic) plume melts formed in the garnet stability field are transferred to the ridge-axis where they mix with MORB melts, bypassing the near-ridge area entirely. The near-axis plume volcanics are mainly formed by melting the residue of this first, deep melting event, revealing a strong trace-element signature of recycled gabbro within the source of the Foundation plume. Similar features are seen in other near-axis hotspot magmas around the world.

The Foundation hotspot track lies in the South Pacific (Figure 1a). For the last 15Ma the Pacific-Antarctic Ridge (PAR) has been slowly approaching the hotspot [9] and at present appears to lie immediately west of it [9]. The approach of the ridge through time has been accompanied by both a change in the style of volcanism (from isolated, approximately conical seamounts in the intraplate region to linear ridges in the near-ridge area (Figure 1a and [10])) and a systematic reduction in volcano size (Figure 1a, b and [10]). Concurrently, the Foundation lavas became both progressively depleted in most mantle-incompatible elements (reaching values even lower than local MORB) and lost their primitive He and Ne isotope signatures

(Figure 1; Table 1 and 2 supplementary data). Sr, Nd and Pb isotope ratios, in contrast, show no equivalent pattern [11].

The most striking difference between the near-axis and on-axis magmas is the lack of any primitive noble gas isotopic signal in the seamount magmas (Fig. 1d). He and Ne of near-axis magmas are indistinguishable from average upper mantle values. On-axis samples show more primitive He and Ne isotopic ratios at the hotspot track intersection, decreasing along-axis southward [12]. This can be explained by mixing of enriched, more degassed melts from the Foundation plume with depleted, less degassed, upper mantle melts. If similar mixing processes were occurring beneath the near-axis seamounts then they should show similar He and Ne isotope patterns, which they do not. To produce He and Ne isotopic patterns showing no evidence of the plume endmember, the He and Ne contents of the plume melt contributing to the near-axis seamount magmas must be lower than those in the on-axis magmas, as the amount of plume material in near-axis magmas is larger or at least similar (as indicated by the Pb isotope values of both systems [11-13]) to that in the on-axis magmas. There are three possible methods to lower He & Ne contents of a melt prior to mixing: (1) Higher melting degrees, (2) magmatic degassing and (3) prior melting leaving a depleted residue. Process one and two can be ruled out for Foundation; For process (1) the dilution produced by increasing the degree of melting, even assuming 90% He loss during degassing subsequent to melting (Figure 2a), is not large enough to reproduce the observed isotope patterns. For (2) the degree of degassing of the near-axis seamount magmas is lower than that observed for the on-axis magmas, as indicated by the $^{4}He/^{40}Ar^{*}$ signatures (Figure 2b) of both settings (because the concentrations of He, Ne and Ar are linked through their distinct production ratios, noble gas relative abundance ratios are a tracer for fractionation processes occurring during magma formation and evolution e.g. [14]. In the case of $^{4}He/^{40}Ar^{*}$, degassing is shown by higher ratios because He is more soluble in basaltic melts than Ar e.g. [14]). Thus, the only feasible process to produce the contrasting He and Ne isotope patterns between near-axis seamount and on-

axis magmas is that primitive plume He and Ne are bypassing the near-ridge area. As this primitive signature can be expected to be carried by the initial melts formed deep in the plume melting column (fertile mantle starts melting at greater depth than upper mantle material feeding mid-ocean ridges e.g. [15-18]), our data suggest that these first melts are being transported directly to the ridge. The decreasing size of the volcanoes (Figure 1a, b and [10]) as the axis is approached (in contrast to expectations of increased melting in an ever-lengthening melt column as the lithospheric lid progressively thins) provides additional evidence that melts are being removed from the near-axis melt column.

A “stripping” of deep plume melts with primitive noble gas isotope ratios to the ridge is also supported by the trace element signatures observed in the near-axis seamounts (Figure 1). Progressive depletion in incompatible-elements in the near-axis volcanoes (termed here "ultradepletion" as incompatible-element ratios are in some cases below those of both local- and N-MORB) is accompanied by the development of positive, fractional-crystallization-independent Sr anomalies and anomalously low Ce/Pb (Figure 3a). Both imply that this ultradepletion is not merely the result of more extensive melting of a lherzolite source. Modeling confirms this, as progressive melting (coloured lines) can neither reproduce the Ba_N/Yb_N vs. Dy_N/Yb_N nor the Ba_N/Yb_N vs. Sr/Sr* variations seen (Figure 3). Simple mixing with local MORB, whilst it could account for the variations seen in magmas with Ba_N/Yb_N >5, cannot produce the ultradepleted, Sr-rich magmas (Figure 3). In Figure 4 we quantify these geochemical changes, defining a depletion factor which is the difference between logs of normalized concentrations of elements in the average ultradepleted magma relative to near-ridge or intraplate averages. A depletion factor of 0 signals no difference in element concentration between the two averages being compared. This is plotted against the bulk solid/melt distribution coefficients of the trace elements during garnet lherzolite melting. Four important features are immediately apparent: (1) the depletions (with the exception Sr, Pb and Cs) are strongly correlated with the bulk Kds; (2) Sr, Pb and to a lesser extent Cs show lower

depletion factors (note that Eu/Eu* shows a strong positive correlation with Sr/Sr* (not shown) but with such a low range (Sr/Sr* varies from 1-3 while Eu/Eu* varies from 1 - 1.1) that the effect is not evident on Figure 4); (3) enrichments in Sr, Eu and Pb (together with depletions in Zr and Hf) are characteristic of modern oceanic gabbros (Figure 4b) and (4) depletion (factor >0) is present even for elements which have Kd>>1 for garnet lherzolite melting. This latter feature is strong evidence (together with Ce/Pb and melt modeling, Figure 3) that partial melting is not controlling the depletion in the near-ridge magmas - partial melting variations with residual garnet would produce incompatible-element patterns which cross near Gd leading to both depletions and enrichments on diagrams like Figure 4.

Evidence of strong Sr- (and often Pb-) enrichment in otherwise relatively depleted magmas has also been reported from other near-ridge hotspots, such as Galapagos [19], Iceland [20] and Easter [21] (see Figure 3 and inset Figure 4). But perhaps most spectacular is the case of Hawaii, which was near-ridge ca. 80 Ma ago when it erupted both enriched and depleted magmas [8], the depleted samples showing strong positive Sr anomalies [22] not attributable to crustal contamination [23]. Such Sr-rich melts are still a part of the Hawaiian plume products today [24], albeit only as melt inclusions in olivine phenocrysts - modern Hawaiian lavas show no discernable Sr-anomaly. This has been attributed to the small volumes of depleted magmas being produced at present, insufficient to influence overall lava Sr contents significantly. There appears to be general consensus (but see [25]) that Sr (and Pb) enrichments are the result of the incorporation of recycled gabbro in the plume source [20,23,24] (see also melting experiments on eclogites derived from oceanic gabbros [23]). This is confirmed by our examination of trace element ratios from modern-day oceanic gabbros (see Figure 1 Supplemental information), which have Sr and Pb anomalies similar to the ultradepleted Foundation magma compositions (Figure 4b). The positive Ba-anomaly seen in some oceanic gabbros is not present in our Foundation magmas, nor are the marked negative Zr and Hf anomalies. Modern gabbros appear always to show Sr and Pb enrichment (>95% of samples

studied, n=126 and 77, respectively) whilst Ba does not always follow suit (68% of samples studied, n=125). We conclude that the absence of a Ba-anomaly at Foundation does not negate the gabbro source model. In the case of Zr and Hf, if initial peridotite melting produces a carbonatite, as seems likely from experiments [26], the residue will be significantly enriched specifically in these elements. Further melting will release them from the source and, when combined with Zr and Hf poor melts from the eclogite, could lead to erupted magmas with no significant Zr or Hf depletion/enrichment. .

We conclude that hotspot magmas erupted close to a spreading axis often show trace element compositions strongly influenced by a gabbro component which, although present in the sources of several if not all hotspots, is so poor in most trace elements that its contribution to magmatism is generally never detected. We suggest that this depleted magma type becomes dominant in a near-ridge setting for two reasons. Firstly, deep melts from the plume are preferentially channeled to the spreading axis. During peridotite melting, the incompatible elements are very strongly partitioned into these initial deep melts, so their removal to the axis leaves a highly incompatible-element depleted peridotitic residuum. Secondly, as the gabbro component will, mineralogically, be present as a clinopyroxene-rich (>75%) eclogite at mantle pressures[23] its trace elements will be retained in the mantle much longer during adiabatic melting (bulk partition coefficients for most incompatible elements >10 times higher for eclogite [23] than for peridotite). So as the lithospheric cap thins and the plume ascends to ever shallower depths, melting more extensively, the eclogitic melts will progressively dominate the pooled melt composition which is erupted. Provided the deep melt extraction to the ridge occurs AFTER the first peridotitic melts have been produced, the gabbro signature should become visible in the erupted magmas even if the eclogite solidus lies deeper[23] than that of fertile peridotite

REFERENCES

[1] Ito, G., Lin, J., and Graham, D. W., Observational and theoretical studies of the dynamics of mantle plume-mid-ocean ridge interaction. *Reviews in Geophysics* **41** (4), 3-1 - 3-24 (2003).

[2] Braun, M. G. and Sohn, R. A., Melt migration in plume-ridge systems. *Earth and Planetary Science Letters* **213**, 417-430 (2003).

[3] Hall, P. S. and Kincaid, C., Melting, dehydration, and the geochemistry of off-axis plume-ridge interaction. *Geochemistry Geophysics Geosystems* **5** (12), doi: 10.1029/2003GC000667 (2004).

[4] Ito, G. and Lin, J., Oceanic spreading centre-hotspot interaction: Constraints from along-isochron bathymetric and gravity anomalies. *Geology* **23**, 657-661 (1995).

[5] Schilling, J.-G., Thompson, G., Kingsley, R., and Humphris, S., Hotspot-migrating ridge interaction in the South Atlantic. *Nature* **313**, 187-191 (1985).

[6] Coffin, M. F. and Gahagan, L. M., Ontong Java and Kerguelen Plateaux: Cretaceous Icelands? *Journal geological Society London* **152**, 1047-1052 (1995).

[7] Haase, K. M., The relationship between the age of the lithosphere and the composition of oceanic magmas: Constraints on partial melting, mantle sources and the thermal structure of the plates. *Earth and Planetary Science Letters* **144**, 75-92 (1996).

[8] Keller, R. A., Fisk, M. R., and White, W. M., Isotopic evidence for Late Cretaceous plume-ridge interaction at the Hawaiian hotspot. *Nature* **405**, 673-676 (2000).

[9] O'Connor, J. M., Stoffers, P., and Wijbrans, J. R., Migration rate of volcanism along the Foundation Chain, SE Pacific. *Earth and Planetary Science Letters* **164**, 41-59 (1998).

[10] Maia, M. et al., The Pacific-Antarctic Ridge-Foundation hotspot interaction: a case study of a ridge approaching a hotspot. *Marine Geology* **167**, 61-84 (2000).

[11] Maia, M., Hémond, C., and Gente, P., Contrasted interactions between plume, upper mantle, and lithosphere: Foundation chain case. *Geochemistry Geophysics Geosystems* **2**, doi: 10.1029/2000GC000117 (2001).

[12] Stroncik, N. A., Niedermann, S., and Haase, K. M., Plume-ridge interaction revisited: Evidence for mixing of melts from He, Ne and Ar isotope and abundance systematics. *Earth and Planetary Science Letters* **268**, 424-432 (2008).

[13] Haase, K. M., Stroncik, N. A., Hekinian, R., and Stoffers, P., Nb-depleted andesites from the Pacific-Antarctic Rise as analogs for early continental crust. *Geology* **33** (12), 921-924 (2005).

[14] Ozima, M. and Podosek, F. A., *Noble gas geochemistry*, 2nd ed. (Cambridge University Press, Cambridge, 2002).

[15] Ito, G. and van Keken, P. E., Hot Spots and Melting Anomalies. *Treatise on Geophysics* **7**, 371-435 (2007).

[16] Bianco, T. A. et al., Geochemical variation at the Hawaiian hot spot caused by upper mantle dynamics and melting of a heterogeneous plume. *Geochemistry Geophysics Geosystems* **9** (11), doi:10.1029/2008GC002111 (2008).

[17] Phipps Morgan, J. and Morgan, W. J., Two-stage melting and the geochemical evolution of the mantle; a recipe for mantle plum-pudding. *Earth and Planetary Science Letters* **170** (3), 215-239 (1999).

[18] Devey, C. W. et al., Giving birth to hotspot volcanoes: distribution and composition of young seamounts from the seafloor near Thahiti and Pitcairn Island. *Geology* **31** (5), 395-398 (2003).

[19] Harpp, K. S. and White, W. M., Tracing a mantle plume: Isotopic and trace element variations of Galapagos seamounts. *Geochemistry Geophysics Geosystems* **2(6)**, doi:10.1029/2000GC000137 (2001).

[20] Chauvel, C. and Hémond, C., Melting of a complete section of recycled oceanic crust: Trace element and Pb isotopic evidence from Iceland. *Geochemistry Geophysics Geosystems* **1**, doi:10.1029/1999GC000003 (2000).

[21] Haase, K. M. and Devey, C. W., Geochemistry of lavas from the Ahu and Tupa volcanic fields, Easter Hotspot, southeast Pacific: Implications for intraplate magma

genesis near a spreading axis. *Earth and Planetary Science Letters* **137**, 129-143 (1996).

[22] Huang, S. and Frey, F. A., Recycled oceanic crust in the Hawaiian plume: evidence from temporal geochemical variations within the Koolau shield. *Contributions to Mineralogy and Petrology* **149** (5) (2005).

[23] Yaxley, G. M. and Sobolev, A. V., High-pressure partial melting of gabbro and its role in the Hawaiian magma source. *Contributions to Mineralogy and Petrology* **154**, 371-383 (2007).

[24] Sobolev, A. V., Hofmann, A. W., and Nikogosian, I. K., Recycled oceanic crust observed in "ghost plagioclase" within the source of Mauna Loa lavas. *Nature* **404**, 986-990 (2000).

[25] Saal, A. E. et al., The role of lithospheric gabbros on the composition of Galapagos lavas. *Earth and Planetary Science Letters* **257** (3-4), 391-406 (2007).

[26] Dasgupta, R. et al., Trace element partitioning between garnet lherzolite and carbonatite at 6.6 and 8.6 GPa with applications to the geochemistry of the mantle and of mantle-derived melts. *Chemical Geology* **262** (1-2), 57-77 (2009).

[27] Stein, C. A. and Stein, S. A., A model for the global variation in oceanic depth and heat-flow with lithospheric age. *Nature* **359**, 123-129 (1992).

[28] Hofmann, A. W., Chemical differentiation of the Earth: the relationship between mantle, continental crust, and oceanic crust. *Earth and Planetary Science Letters* **90**, 297-314 (1988).

[29] Graham, D. W., in *Noble gases in geochemistry and cosmochemistry*, edited by D. Porcelli, C. J. Ballentine, and R. Wieler (2002), Vol. 47, pp. 247-317.

[30] Haase, K. M., Devey, C. W., and Goldstein, S. L., Two-way exchange between the Easter mantle plume and the Easter microplate spreading axis. *Nature* **382**, 344-346 (1996).

ACKNOWLEDGEMENTS

We thank D. Ackermand, B. Mader and D. Garbe-Schönberg (Institut für Geowissenschaften, University of Kiel) for help with the major and trace element analyses; S. Niedermann (GFZ Potsdam) provided extensive support for the noble gas analyses. Ben Holtzman, Bill White, Dennis Geist and several anonymous reviewers provided constructive comments on earlier versions of the manuscript which helped to improve this paper greatly. Sampling was carried out with research vessel “Sonne” financed by the German Ministry of Science and Technology (BMBF).

Corresponding Author: Nicole Stroncik, to whom requests for material should be made

Author contributions: NS was responsible for noble gas analyses, CWD supervised trace element analyses. Both authors worked equally on writing and revising the paper and developing the ideas it contains.

FIGURE CAPTIONS

Figure 1: Variations in bathymetry (a) and magma composition (b-d) along the Foundation Seamount chain. Height of individual volcanoes as difference between summit depth and theoretical depth based on plate cooling model [27], Ba/Yb ratios normalised to NMORB [28]. $^{3}He/^{4}He$ and $^{21}Ne/^{22}Ne$ ratios measured on fresh glass and olivine separates, typical MORB values from ref. [29]. Fresh glass or olivine was not found in samples erupted >200km from the axis. The most westerly "Near-axis seamount" (larger symbol) sample gives the best approximation we have of the hotspot He and Ne isotopic ratios [12]. 2σ uncertainties are shown where larger than symbol.

Figure 2: $^{206}Pb/^{204}Pb$ plotted against (a) $^{4}He/^{3}He$ and (b) $^{4}He/^{40}Ar^{*}$ ($^{40}Ar^{*}$ is measured ^{40}Ar corrected for atmospheric contamination as described in Graham [29]). Data from suppl. Table 1 and 2 and [11]. Coloured lines represent different melting and mixing models (model details are explained in “ModelDetails.doc” supplementary data). The two larger symbols represent age corrected data (see “ModelDetails.doc” supplementary data). 2σ uncertainties are shown where larger than symbol.

Figure 3: MORB[28] normalized (N) variations of Ba_N/Yb_N versus (a) Sr-anomaly (calculated as the $Sr_N/\sqrt{(Pr_N \cdot Nd_N)}$), (b) Dy_N/Yb_N (sensitive to the presence of residual garnet during melting). Coloured fields labeled "intraplate", "near-ridge" and "ultradepleted" enclose samples averaged for the geochemical modeling shown in Figure 4. Lines show mixing between "intraplate" and "near-ridge" (black) and melting in the spinel (red) or garnet (blue) stability field (model details are explained in “ModelDetails.doc” supplementary data).

Figure 4: Modeling of trace element depletion. (a) Depletion factor (= $\log(X_{Na})$-$\log(X_{Nb})$, where X_N = MORB-normalized concentration of element, a and b = either "near-ridge" and "ultradepleted" (purple symbols) or "intraplate" and "ultradepleted" (red)) against bulk partition coefficients for garnet lherzolite melting (see supplementary information). Inset: similar diagram for young Easter Seamounts lavas (data field [21,30] shown in Figure 3) and

277 Galapagos (compiled from the GEOROC database Mainz) comparing averages with
278 $Ba_N/Yb_N>10$ (equivalent to "intraplate") and Sr/Sr*>2 (equivalent to "ultradepleted"). (b)
279 Trace element patterns of average ocean floor gabbro (compiled from the PetDB database)
280 and the Foundation magmatic groups.

281

282

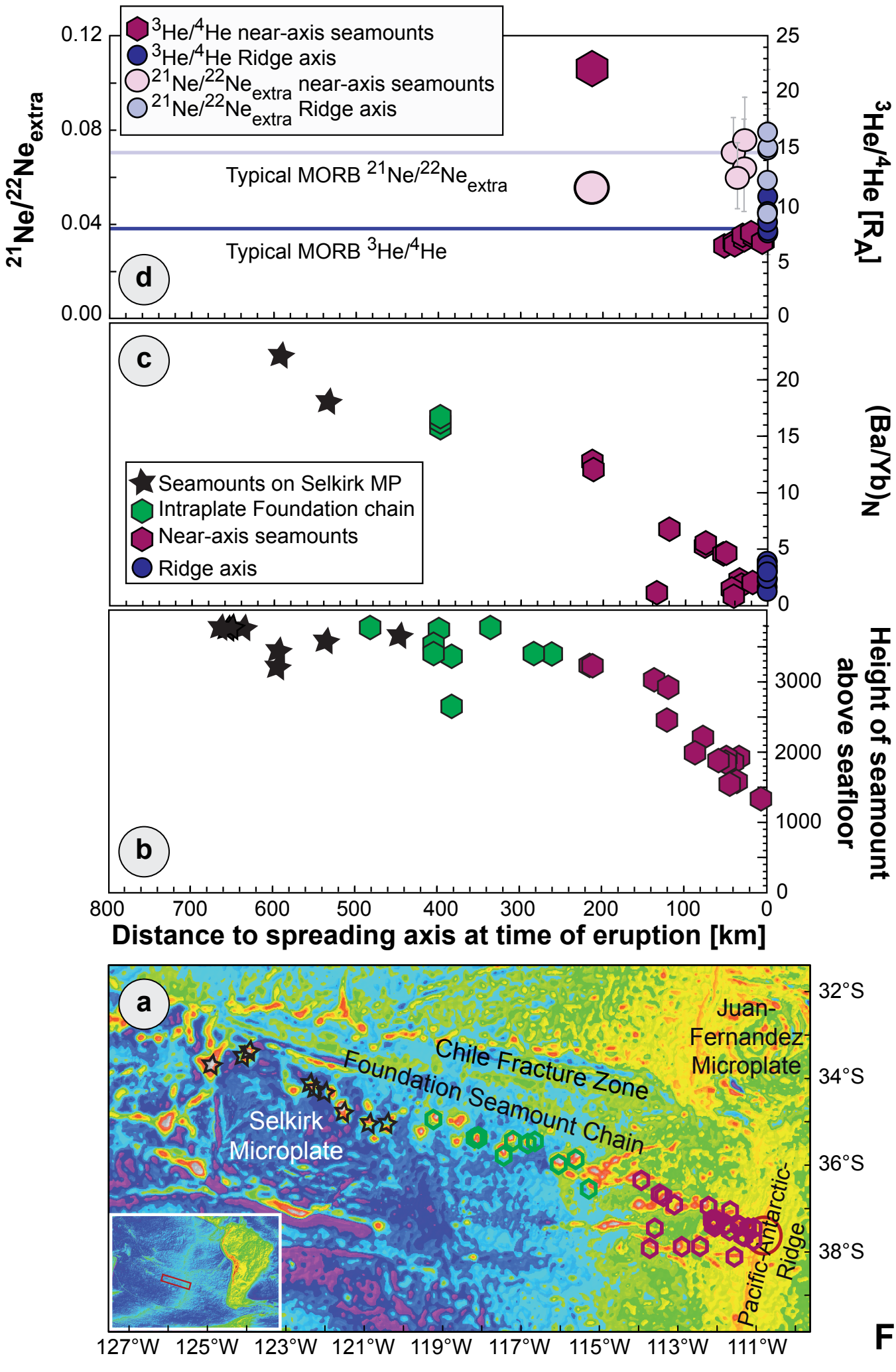
^{3}He/^{4}He near-axis seamounts
^{3}He/^{4}He Ridge axis
^{21}Ne/^{22}Ne$_{extra}$ near-axis seamounts
^{21}Ne/^{22}Ne$_{extra}$ Ridge axis
Typical MORB ^{21}Ne/^{22}Ne$_{extra}$
Typical MORB ^{3}He/^{4}He
d
c
b
a
Seamounts on Selkirk MP
Intraplate Foundation chain
Near-axis seamounts
Ridge axis
^{21}Ne/^{22}Ne$_{extra}$
^{3}He/^{4}He [R$_A$]
(Ba/Yb)$_N$
Height of seamount above seafloor
Distance to spreading axis at time of eruption [km]
Chile Fracture Zone
Foundation Seamount Chain
Selkirk Microplate
Juan-Fernandez Microplate
Pacific-Antarctic-Ridge
32°S
34°S
36°S
38°S
127°W
125°W
123°W
121°W
119°W
117°W
115°W
113°W
111°W

Fig. 1

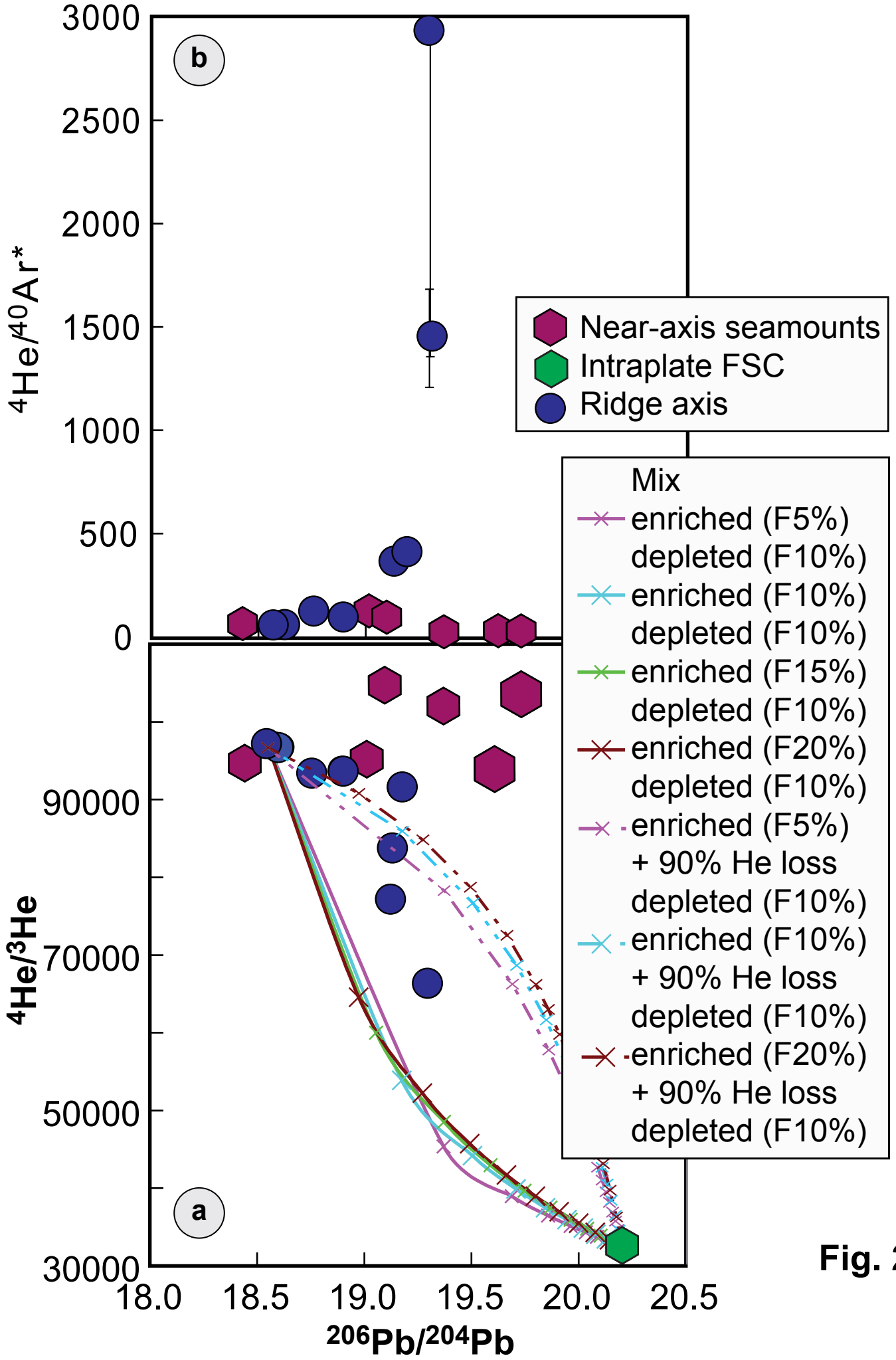
b
a
3000
2500
2000
1500
1000
500
0
$^4He/^{40}Ar^*$
90000
70000
50000
30000
$^4He/^3He$
18.0
18.5
19.0
19.5
20.0
20.5
$^{206}Pb/^{204}Pb$
Near-axis seamounts
Intraplate FSC
Ridge axis
Mix
enriched (F5%)
depleted (F10%)
enriched (F10%)
depleted (F10%)
enriched (F15%)
depleted (F10%)
enriched (F20%)
depleted (F10%)
enriched (F5%)
+ 90% He loss
depleted (F10%)
enriched (F10%)
+ 90% He loss
depleted (F10%)
enriched (F20%)
+ 90% He loss
depleted (F10%)

Fig. 2

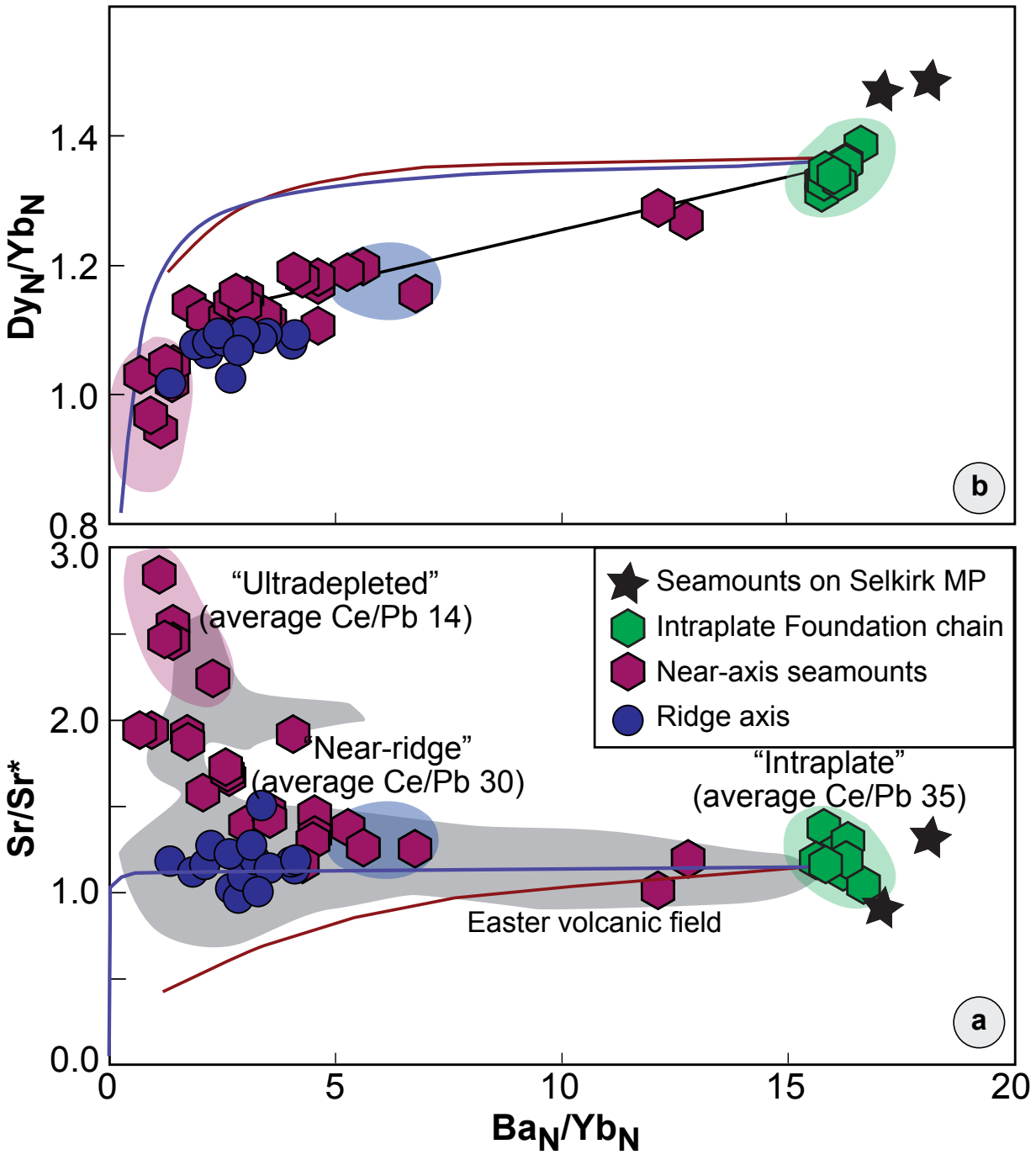
1.4
1.2
1.0
0.8
Dy_N/Yb_N
b
3.0
2.0
1.0
0.0
Sr/Sr^*
"Ultradepleted"
(average Ce/Pb 14)
"Near-ridge"
(average Ce/Pb 30)
"Intraplate"
(average Ce/Pb 35)
Easter volcanic field
Seamounts on Selkirk MP
Intraplate Foundation chain
Near-axis seamounts
Ridge axis
a
0
5
10
15
20
Ba_N/Yb_N

Fig. 3

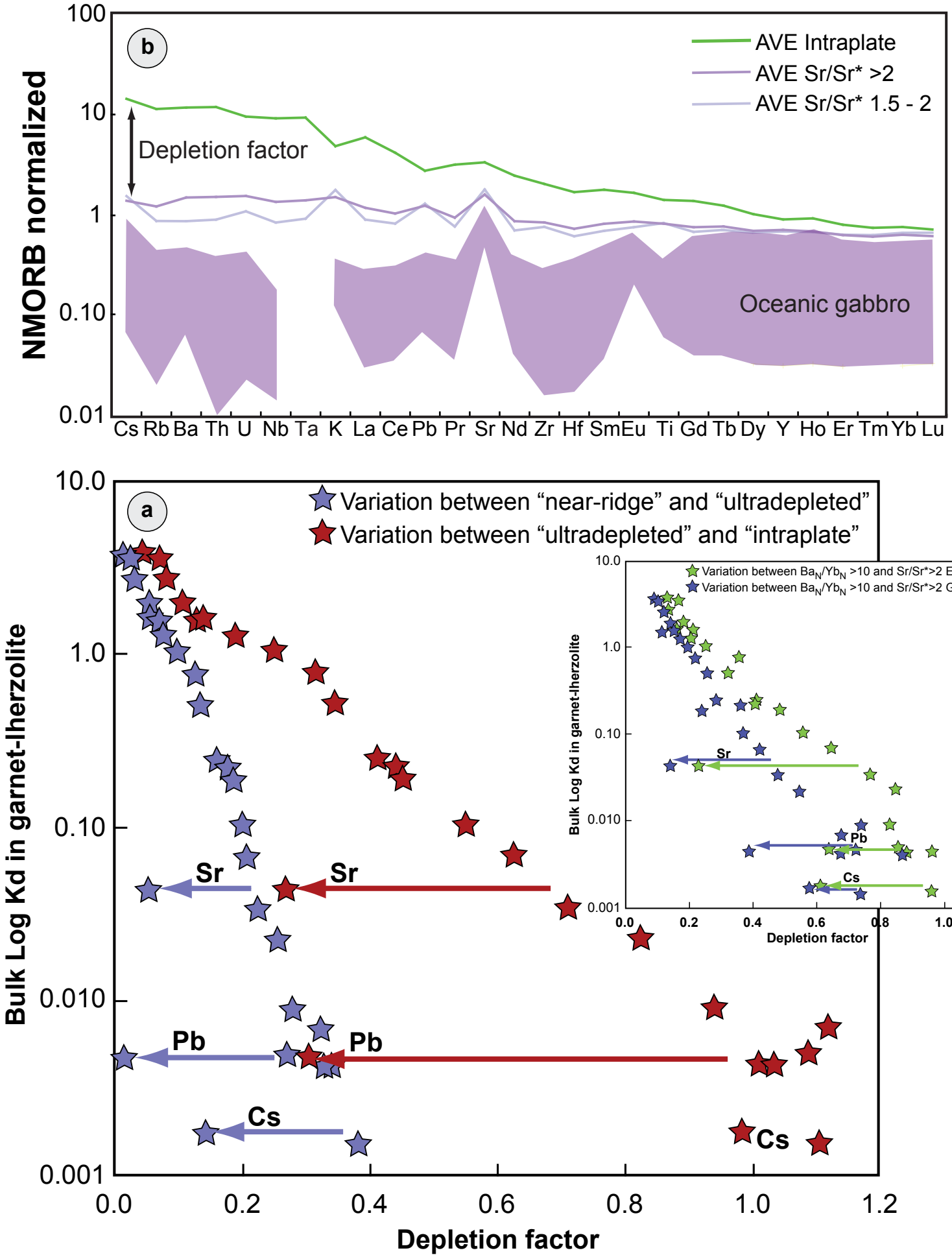
b
AVE Intraplate
AVE Sr/Sr* >2
AVE Sr/Sr* 1.5 - 2
Depletion factor
Oceanic gabbro
NMORB normalized
100
10
1
0.10
0.01
Cs Rb Ba Th U Nb Ta K La Ce Pb Pr Sr Nd Zr Hf Sm Eu Ti Gd Tb Dy Y Ho Er Tm Yb Lu
a
Variation between "near-ridge" and "ultradepleted"
Variation between "ultradepleted" and "intraplate"
Sr
Sr
Pb
Pb
Cs
Cs
Bulk Log Kd in garnet-lherzolite
Depletion factor
10.0
1.0
0.10
0.010
0.001
0.0
0.2
0.4
0.6
0.8
1.0
1.2
Variation between Ba_N/Yb_N >10 and Sr/Sr*>2 ESC
Variation between Ba_N/Yb_N >10 and Sr/Sr*>2 Galapágos
Sr
Pb
Cs
Bulk Log Kd in garnet-lherzolite
Depletion factor

Fig. 4